MRS Advances © 2019 Materials Research Society
DOI: 10.1557/adv.2019.445

X-Ray Dynamical Diffraction in Powder Samples with Time-Dependent Particle Size Distributions

Adriana Valério[1], Sérgio L. Morelhão[1], Alex J. Freitas Cabral[2;3], Márcio M. Soares[4], and Cláudio M. R. Remédios[2]

[1]*Institute of Physics, University of São Paulo, São Paulo 05508-090, Brazil*

[2]*Instituto de Ciências Exatas e Naturais, Universidade Federal do Pará, Belém, PA, Brazil*

[3]*Universidade Federal do Oeste do Pará, Santarém, PA, Brazil*

[4]*Laboratório Nacional de Luz Síncrotron - LNLS/CNPEM, Campinas, SP, Brazil*

ABSTRACT

In situ X-ray diffraction is one of the most useful tools for studying a variety of processes, among which crystallization of nanoparticles where phase purity and size control are desired. Growth kinetics of a single phase can be completely resolved by proper analysis of the diffraction peaks as a function of time. The peak width provides a parameter for monitoring the time evolution of the particle size distribution (PSD), while the peak area (integrated intensity) is directly related to the whole diffracting volume of crystallized material in the sample. However, to precisely describe the growth kinetics in terms of nucleation and coarsening, the correlation between PSD parameters and diffraction peak widths has to be established in each particular study. Corrections in integrated intensity values for physical phenomena such as variation in atomic thermal vibrations and dynamical diffraction effects have also to be considered in certain cases. In this work, a general correlation between PSD median value and diffraction peak width is deduced, and a systematic procedure to resolve time-dependent lognormal PSDs from in situ XRD experiments is described in details. A procedure to correct the integrated intensities for dynamical diffraction effects is proposed. As a practical demonstration, this analytical procedure has been applied to the single-phase crystallization process of bismuth ferrite nanoparticles.

INTRODUCTION

Advanced synchrotron sources of high flux combined with detector systems capable of collecting, in just a few seconds, full X-ray diffraction (XRD) patterns of powder samples create opportunities for in situ studies of a variety of processes such as catalysis [1,2], energy storage and conversion [3], and crystallization of nanoparticles from amorphous precursors [4,5]. Fast in situ data acquisition may result in thousands of XRD patterns containing information on structural changes along the processes. Particularly in crystallization studies, there will be information on crystalline phases, lattice strain, and particle size distribution (PSD) as a function of time and temperature, covering the whole process from amorphous to fully crystalline phases.

Besides position of the diffraction peaks that can provide information on thermal expansion coefficients from nanoscale to large particles with bulk properties, width and area of the diffraction peaks allow detailed investigation of the growth kinetics, evidencing the role of nucleation and coarsening in time-dependent PSDs. Particle size from diffraction peak widths stand for just one value that can be produced by countless PSDs. In situ measures of integrated intensities during growth of crystalline particles provide a direct route to access fluctuation in the population $N(t)$ of particles as a function of time t. Stages of nucleation, $dN/dt > 0$, and coarsening (particles growing in size) can be resolved from the experimental integrated intensities when compared to theoretical values for PSDs with constant number of particles and with imposed constraints to the determined particle sizes from diffraction peak widths. Coarsening under constant volume of diffraction is possible at the cost of small particles that are dissolved, $dN/dt < 0$, providing material to the larger ones in a process widely known as the Ostwald ripening phenomenon. Since first described by Wilhelm Ostwald in 1896, the phenomenon has been observed in a number of general nanocrystal growth systems where broad spectrum of particle sizes is present [6]. This process play a fundamental role in determining the evolution in time of the particle population, and it is crucial in controlling size and size distribution during synthesis of nanocrystals.

For PSDs with broader distributions, particle sizes from diffraction peak widths have complex behavior with the PSD parameters such as mode (most probable value) and standard deviation, and where dynamical diffraction corrections can be indispensable. For strong Bragg reflections, neglecting dynamical corrections in broad PSDs with many particles of sizes above a few hundred nanometers leads to incorrect reading of the PSD parameters. The large-particle kinematical intensity contributions are much stronger than they actually are when neglecting dynamical effects. Then, the mode and width of the PSDs would have to be smaller than their actual values to reproduce the experimental peak widths. In this work we developed a systematic procedure to resolve time-dependent PSDs for in situ XRD studies. It is based on the kinematical approach of X-ray diffraction [7], with proper integrated reflectivity corrections from dynamical diffraction calculation [8]. As practical demonstration, the calculation involved in this analytical procedure is carried out for the single-phase crystallization process of bismuth ferrite [9].

X-RAY DIFFRACTION IN PARTICLE SIZE DISTRIBUTIONS

According to the kinematical theory of X-ray diffraction, the integrated intensity $P_c = \int I_c(2\theta) d2\theta$ or area under each diffraction peak $I_c(2\theta)$ from a single crystallite (small crystal, grain, or particle diffracting in powder samples) as a function of the scattering angle 2θ is proportional to the crystallite volume V_c, that is $P_c \propto V_c$ [4]. On the other hand, while the peak area increase with V_c, the peak width (fwhm – full width at

half maximum) β gets narrower inversely with crystallite size L, that is $\beta \propto 1/L$. To account for the fact that actual powder samples are formed by crystallites with different sizes, the number of diffracting particles (crystallites) with size between L and $L + dL$ is given by $n(L)dL$ where $n(L)$ is the particle size distribution (PSD) function so that

$$N = \int n(L)dL \qquad (1)$$

is the total number of diffracting particles in the sample.

By using normalized line profile functions, such as a Lorentzian

$$\mathcal{L}(2\theta) = \beta^2/[4(2\theta - 2\theta_B)^2 + \beta^2], \qquad (2)$$

crystallites of size L produce a diffraction peak

$$I_c(L, 2\theta) = K\, V_c(L)\, A^{-1}(\beta)\, \mathcal{L}(2\theta) \qquad (3)$$

where K contains all terms that are independent of the crystallite size for reflections of Bragg angle θ_B. It provides diffraction peaks of fwhm β and integrated intensity $P_c = \int I_c(L, 2\theta)d2\theta = K\, V_c(L)$, since $\int \mathcal{L}(2\theta)d2\theta = A(\beta)$. For the line profile function in Equation (2), $A(\beta) = \pi\beta/2$, and in the case of crystallites with cubic shape of edges L, $V_c(L) = L^3$ and the fwhm $\beta \approx 0.92\lambda/L\cos\theta_B$ follows from Scherrer equation (SE) [10]. Diffraction peaks from the powder samples are then given by

$$I(2\theta) = \int I_c(L, 2\theta)\, n(L)dL, \qquad (4)$$

whose integrated intensity $P = \int I(2\theta)d2\theta = K\int V_c(L)\mathrm{n}(L)dL = KV$ are proportional to the total volume V of diffracting particles.

Measurable diffraction peaks of powder samples with PSD have width β_s defined at the half maximum according to

$$I(2\theta_B \pm \beta_s/2) = \tfrac{1}{2}\int I_c(L, 2\theta_B)n(L)dL = \int_0^{L_s} I_c(L, 2\theta_B)n(L)dL \qquad (5)$$

where the median value L_s is related to the fwhm β_s through the SE (to be numerically demonstrated later on). It means that the experimental peak widths lead to the median value L_s of the intensity-weighted PSD, that is weighting by the particles' dimension to the power of four as from Equation (3) we have $I_c(L, 2\theta_B)n(L)dL \propto L^4 n(L)dL$.

DYNAMICAL DIFFRACTION CORRECTIONS

In a crystal slab of thickness L', the integrated reflectivity $R_{dyn}(L')$ from dynamical diffraction calculation in specular reflection geometry is always smaller than a finite value and it is proportional to L' within the kinematical approach, only for very small crystals [11-13]. In more precise words,

$$\lim_{L'\to\infty} R_{dyn}(L') < W \text{ and } \lim_{L'\to 0} R_{dyn}(L') = \alpha L'$$

where W is the intrinsic width [14,15] of a Bragg reflection and α is just a constant of proportionality. Examples of dynamical integrated reflectivities [7], $R_{dyn}(L')$, in $BiFeO_3$ (BFO) crystals are shown in Figure 1.

To account for dynamical diffraction corrections or, as formerly called, primary extinction, the diffraction peak expression for crystallites of size L in Equation (3) can be multiplied by the ratio $R_{dyn}(L')/\alpha L'$ having in mind that L' stands for the crystallite dimension along the normal direction of the Bragg planes. In the case of cubic crystallites of edge L and Bragg planes parallel to one face of the crystallites, dynamical diffraction effects are easily taking into account by rewriting Equation (3) as

$$I_c(L, 2\theta) = K\,\alpha^{-1} R_{dyn}(L) L^2\, A^{-1}(\beta)\mathcal{L}(2\theta), \qquad (6)$$

in agreement with the kinematical approach where $\int I_c\,(L, 2\theta) d2\theta = KV_c(L)$ when $L \to 0$.

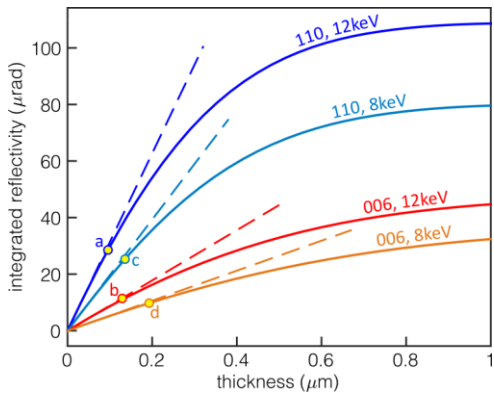

Figure 1. Integrated reflectivities (solid lines) from dynamical diffraction calculation as a function of thickness in BFO crystal slabs. X-rays of 12 keV and 8keV for Bragg reflections 110 and 006. Deviations of 5% from the linear behaviour (dashed lines) due to dynamical diffraction effects (absorption and re-scattering processes) occur for slabs of thicknesses (a) 95.3 nm, (b) 127.9 nm, (c) 136.3 nm and (d) 194,4 nm.

LOGNORMAL PSD

Numerical demonstration of the correlation between β_s and L_s in Equation (5) through the SE is carried out here for the case of the most used function describing PSD in powder samples, which is the lognormal PSD [16,17]

$$n(L) = \frac{N}{L\sigma\sqrt{2\pi}} \exp\left[-\frac{(\ln L - \ln L_h)^2}{2\sigma^2}\right]. \qquad (7)$$

$L_h = L_0 \exp(\sigma^2)$ is the median value of the PSD, that is $\int_0^{L_h} n(L)dL = N/2$, given in terms of both PSD parameters, the most probable particle size L_0 (mode) and σ (the standard deviation in log scale). Besides the median value, the PSD width $2L_0 \sinh[\sigma\sqrt{2\ln(2)}]$ at half maximum also depends on both parameters L_0 and σ. It follows from Equation (5) that, in the case of narrow PSDs where $I_c(L, 2\theta_B) n(L) dL \approx I_c(L_0, 2\theta_B) \int n(L) dL$, measures of diffraction peak widths in powder samples provide the particle size $L_s \approx L_h$, see Figure 2(a). For broader PSDs, the particle size L_s obtained from SE has a more complex behavior with the variables L_0 and σ, and where dynamical

diffraction corrections can be indispensable, as shown for instance in Figure 2(b). For strong Bragg reflections such as the 110 reflection in BFO crystals, neglecting dynamical corrections in broad PSDs with many particles of sizes above a few hundred nanometers leads to a deviation from the actual median value. Without accounting for dynamical effects to suppress the kinematical intensity contribution of large particles, the mode and width of the PSDs would have to be much smaller than they actually are to reproduce the experimental peak widths.

In powder samples, measures of x-ray diffraction peak widths β_s provide $L_s = 0.92\,\lambda/\beta_s \cos\theta_B$ (SE for cubic crystallite), corresponding exactly to the median values of the peak intensity distributions defined in Equation (5). This correlation is numerically demonstrated in Figure 3(a), taking as a reference the 110 reflection of the BFO crystal. Diffraction peaks $I(2\theta)$ are simulated by using Equation (4) with the Lorentzian line profile function given in Equation (2), and cubic crystallites with dynamical corrections as in Equation (6). Examples of two simulated diffraction peaks are shown in Figure 3(b). Note that diffraction peak widths are unable to solve both parameters of the PSDs, for a single median value L_s there are countless combinations of L_0 and σ, as shown in the case of the two simulated peaks in Figure 3(b). However, according to Figure 3(a), for a given σ value there is a nearly linear relationship connecting the measured L_s values from diffraction peaks to the PSD mode L_0, e.g., $L_0 = 0.825\,L_s$ for $\sigma = 0.2$. This is an important observation that can be used to monitor time-dependent PSDs via diffraction peak width during in situ studies of crystallization processes.

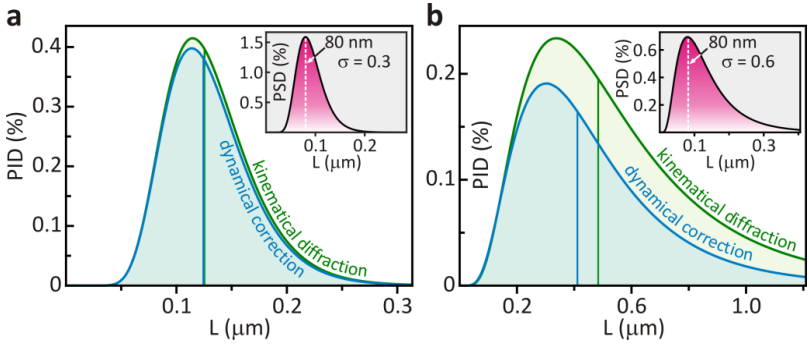

Figure 2. (a,b) Peak intensity distributions (PID) as $I_c(L, 2\theta_B)n(L)dL \propto L^4 n(L)dL$, for lognormal PSDs (insets) with mode L_0 = 80 nm and standard deviation (a) σ = 0.3 and (b) σ = 0.6. Dynamical diffraction corrections, Equation (6), of the kinematical approach in Equation (3) start to be significant in PSDs with sizes above 100 nm. Median values are indicated by vertical lines. Reflection 110 of the BFO crystal with x-rays of 12 keV.

NUCLEATION AND COARSENING

At the very early beginning of the crystallization process, particles are quickly formed at many nucleation sites with narrow size distribution [18]. If X-ray diffraction can already be detected at this early stage, $N_0 = N(t_0)$ is the initial particle population observed at the reference time instant t_0. After this instant, nucleation may simply end or continue followed or not by coarsening. Nucleation without coarsening is easily evidenced by increasing of integrated intensities (peak areas) while diffraction peak widths display nearly constant values as a function of time. To distinguish the instant

when nucleation ends and Ostwald ripening begins, it is necessary to choose a suitable time-dependent PSD to each system under investigation. Lognormal PSD is a reasonable choice as it broads with its mode L_0 even when parameter σ is kept constant. Then, diffraction peak width can be used to monitor the PSD as a function of time. Nucleation rate, end of nucleation, coarsening, and beginning of Ostwald ripening are readily identified by comparing the experimental integrated intensities with the theoretical ones for PSDs with constant population of N_0 particles. In other words, $N(t)/N_0 = P_e(t)/P_0(t)$ where $P_e(t)$ is an experimental integrated intensity and $P_0(t)$ is the integrated intensity calculated for a population of N_0 particles whose PSD $n(t, L)$ is constrained to the $L_s(t)$ values determined from diffraction peak widths.

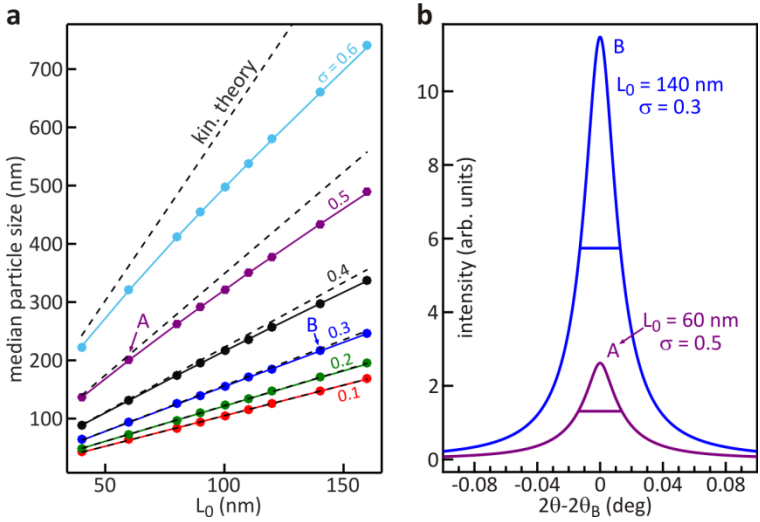

Figure 3. (a) Median particle size L_s (solid lines) according to Equation (5) for different lognormal PSDs of mode L_0 and standard deviation σ, as indicated. Particle sizes from SE (dots) in simulated x-ray diffraction peaks from Equation (4) showing an exact match with the L_s values in Equation (5). Dynamical diffraction effects are disregarded in the kinematical approach (dashed lines, kin, theory). (b) Examples of simulated diffraction peaks I(2θ) of similar widths (horizontal lines) for PSDs with different parameters L_0 and σ (arrows A and B in (a)). Reflection 110 of the BFO crystal with X-rays of 12 keV ($2\theta_B = 21.346°$ at 25°C [19]).

CONCLUSIONS

We show with this work that the peak width appearing in the Scherrer equation stands for the median value of the peak intensity distribution, corresponding to the weighted particle size distribution by particles' dimensions to the power of four in the case of particles with 3D shapes as cubes and spheres. Establishing a direct correlation between diffraction peak width and particle size distribution allows tracking the temporal evolution of the particle size distribution from experimental values of diffraction peak area and width. When compared with theoretical diffraction peak area it's conceivable to distinguish stages of nucleation, coarsening, and Ostwald ripening. Moreover, applying dynamical corrections can be relevant depending on X-ray energy, chosen reflection, material, and mainly on size of the largest particles present in a given distribution.

REFERENCES

[1] A. Vamvakeros, S. D. M. Jacques, M. Di Michiel, et al. Nat Commun. 9, 4751 (2018).
[2] Ying-Qiu Gu, Xin-Pu Fu, Pei-Pei Du, et al. J. Phys. Chem. C 119, 17102-17110 (2015).
[3] S.-M. Bak, Z. Shadike, R. Lin, X. Yu, X.-Q. Yang. NPG Asia Materials 10, 563–580 (2018).
[4] J.-L. Mi, T. N. Jensen, M. Christensen, C. Tyrsted, J. E. Jørgensen, B. B. Iversen. Chem. Mater. 23, 1158–1165 (2011).
[5] G. Clarke, A. Rogov, S. McCarthy et al. Scientific Reports 8, 10473 (2018).
[6] Z. Zhang, Z. Wang, S. He, C. Wang, M. Jin, and Y. Yin, Chem. Sci. 6, 5197 (2015).
[7] S. L. Morelhão, Computer Simulation Tools for X-ray Analysis. (Graduate Texts in Physics Springer, Cham, 2016).
[8] G. Dina, A. G. Gonzalez, S. L. Morelhão, S. Kycia. MRS Advances 3, 2347-2352 (2018).
[9] A. J. Freitas Cabral, A. Valerio, S. L. Morelhão, M. M. Soares, C. M. R. Remedios. To appear in Cryst. Growth & Design (2019).
[10] P. Scherrer. Nachr. Ges. Wiss. Göettingen, Math.-Phys. Kl, 98 (1918).
[11] S. L. Morelhão, C. M. R. Remédios, R. O. Freitas, A. O. dos Santos. J. Appl. Cryst. 44, 93-101 (2011).
[12] S. L. Morelhão, L. H. Avanci. Acta Cryst. A 57, 192-196 (2001).
[13] L. H. Avanci, M. A. Hayashi, L. P. Cardoso, S. L. Morelhão, F. Riesz, K. Rakennus, T. Hakkarainen. J. Cryst. Growth 188, 220-224 (1998).
[14] Integrated reflectivities in semi-infinite crystals (infinite thickness) have maximum values smaller than the intrinsic width W of each Bragg reflection. It follows from the fact that reflectivity curves are always limited to values smaller than 1 hence their area $A < 1 \times W$.
[15] $W = r_e\lambda^2|F_{hkl}F_{\overline{hkl}}|^{1/2}/V_{cell}\sin 2\theta_B$ for σ-polarized x-rays where $r_e = 2.818 \times 10^{-5}$Å is the classic electron radius, F_{hkl} is the structure factor of the hkl reflection with Bragg angle θ_B for the wavelength λ, and V_{cell} is the unit cell volume [7].
[16] L. B. Kiss, J. Söderlund, G. A. Niklasson, C. G. Granqvist. Nanotechnology 10, 25-28 (1999)
[17] A. Cervellino, C. Giannini, A. Guagliardi, M. Ladisa. Phys. Rev. B 72, 035412 (2005).
[18] M. Bruno. CrystEngComm 21, 4918-4924 (2019).
[19] A. Palewicz, R. Przeniosło, I. Sosnowska, A. W. Hewat. Acta Cryst. B 63, 537-544 (2007).